



Investigation of water signatures at gully-exposed sites on Mars by hyperspectral image analysis

Chaojun Fan^{a,*}, Dirk Schulze-Makuch^a, Hongjie Xie^b, Ning Lu^b

^a School of Earth and Environmental Sciences, Washington State University, Pullman, WA 99163, USA

^b Laboratory for Remote Sensing and Geoinformatics, University of Texas at San Antonio, San Antonio, TX 78249, USA

ARTICLE INFO

Article history:

Received 31 October 2007

Received in revised form

24 October 2008

Accepted 26 October 2008

Available online 27 November 2008

Keywords:

Mars

Gully

Water signature

Hyperspectral image

Absorption depth

ABSTRACT

High-resolution images from the Mars Orbiter Camera (MOC) onboard the Mars Global Surveyor (MGS) show a variety of gully features on sloped surfaces of Mars. The mechanism of gully formation is still under debate, although a majority of studies tend to favor a mechanism related to liquid water flow based on geomorphology and fluid mechanics considerations. In this study, we examined four known gully sites using Visible and Infrared Mineralogical Mapping Spectrometer (OMEGA) imagery. In particular, we analyzed the absorption depths of the water-associated absorption bands and concluded that there are stronger water signatures at the gully-exposed sites than in the surrounding areas. This implies that the water signatures, most likely representing water ice, isolated water molecules, and/or hydroxyl molecules incorporated into minerals, are still present in the shallow unconsolidated soils. This study provides additional evidence that water was likely involved in the formation of the gully features and is still locally active on the Martian surface in the present time.

© 2008 Elsevier Ltd. All rights reserved.

1. Introduction

Mars has experienced wet and possible warm surface conditions in its early history (e.g., Sagan et al., 1973; Pollack et al., 1987; Squyres and Kasting, 1994; Golombek, 1999; Tanaka, 2000; Craddock and Howard, 2002; Kerr, 2003; Paige, 2005; Poulet et al., 2005; Bibring et al., 2006; Fan et al., 2008). Localized liquid water activities are thought to have occurred episodically over most of Martian history (Malin and Edgett, 2000a; Christensen, 2003; McCollom and Hynek, 2005; Schulze-Makuch et al., 2007; Soare et al., 2007), up to very recent geologic time (e.g., Malin et al., 2006). The wet and warm conditions of early Mars imply that life might have emerged, and may still be present on Mars (Schulze-Makuch and Irwin, 2004). Thus, any site associated with liquid water may also harbour the potential for life on Mars.

The hydrologic history of Mars has been reconstructed from a variety of indicators, which include: (1) geomorphology such as shorelines, gullies, channels, valleys, and alluvial fans (e.g., Parker et al., 1989; Malin and Edgett, 2000a, 2003; Fairén, et al., 2003; Mangold et al., 2004; Solomon et al., 2005); (2) sedimentary structures such as layered deposits, cross bedding, and layered evaporites (e.g., Malin and Edgett, 2000b; Paige, 2005; Gendrin et al., 2005; Bibring et al., 2005); (3) mineralogy such as hydrated

phyllosilicates, hydrated sulphates, and other hydroxide minerals (e.g., Arvidson et al., 2005; Poulet et al., 2005; Langevin et al., 2005; Bibring et al., 2006); and (4) anomalies of volatile element concentrations such as Br and Cl (e.g., Dreibus and Waenke, 1987, 2000; Squyres et al., 2004; Haskin et al., 2005).

Gullies imaged by the Mars Orbiter Camera (MOC) (1.5–12.0 m/pixel) aboard the Mars Global Surveyor (MGS) were first described by Malin and Edgett (2000a). The gully features have been found on crater walls, valley walls, polar pits, scarp faces, mesas, and fretted terrain mostly in areas of 30–72° latitude in both hemispheres (Heldmann and Mellon, 2004). A gully-exposed site may consist of a single gully or more commonly a gully system with tens of gullies occurring side by side on the same slope face. A single gully is composed of an alcove, a main V-shape channel, and depositional aprons. This is referred to as the alcove-channel-apron structure, which can be hundreds of meters to a few kilometres in length (Heldmann et al., 2007).

Several mechanisms have been proposed to explain the gully formation. These can be summarized into two categories: liquid water-related and non-liquid water related. The proposed liquid water mechanisms include: (1) groundwater seeping out onto the surface (i) from a shallow subsurface aquifer (Malin and Edgett, 2000a; Mellon and Phillips, 2001; Heldmann and Mellon, 2004; Heldmann et al., 2005, 2007), (ii) from a deep subsurface aquifer (Gaidos, 2001), or (iii) via localized geothermal heating of permafrost ice (Hartmann, 2001); (2) water melting from shallow ground ice at high obliquity (Costard et al., 2002); and (3) snowmelt from dissipating snow packs at high obliquity

* Corresponding author. Tel.: +1 509 335 9185; fax: +1 509 335 7816.

E-mail addresses: cfan@mail.wsu.edu, chaojunfan.fan@gmail.com (C. Fan), dirksm@wsu.edu (D. Schulze-Makuch), Hongjie.Xie@utsa.edu (H. Xie).

(e.g., Christensen, 2003). The non-liquid water mechanisms include: (1) liquid CO₂ from a buried reservoir (Musselwhite et al., 2001); (2) liquid hydrocarbon seepage (Direito and Webb, 2007); (3) dry landslides (Treiman, 2003); (4) dust avalanches (Sullivan et al., 2001); and (5) windy sand dune activity (Bart, 2007).

Heldmann et al. (2007) examined gullies and associated mechanisms in detail and suggested that a liquid water mechanism is most likely. The suggested water source would be seepage and surface runoff of groundwater from shallow aquifers due to the melting-freezing cycles of ice-cemented soil plugs between the aquifer and the slope surface. This process would be induced by obliquity change of Mars or by localized geothermal heating in recent geologic time. Malin et al. (2006) compared MOC images taken in December 2001 and April 2005 for one site and in August 1999 and February 2004 for another site, and concluded that these sites exhibited evidence for liquid water activity in the past few years.

The formation mechanisms of these features, especially in relation to the fluid agent, have been discussed primarily based on geomorphology and fluid mechanics. Our hypothesis is that if liquid water has been the fluid agent, then we should be able to detect water signatures by using hyperspectral images. Liquid water movement near the subsurface would most likely be associated with (1) fast evaporation of water into the atmosphere; (2) freezing of water in the pore space of loose materials; or (3) incorporation of water into minerals by chemical alteration. If so, the gully-exposed sites are likely to maintain more water than their surrounding areas if the gullies were generated by liquid water, especially for those gullies formed recently. This “wetter” surface (sand, soil, and regolith) could then be detected with reflectance spectral images.

Hyperspectral images in visible and infrared wavelengths were obtained from OMEGA on board the ESA/Mars Express. The spacecraft began to take images in 2003 and operates within the wavelength range 0.35–5.2 μm using 352 spectral bands of 7 to 20 nm spectral resolution. OMEGA provides images at a spatial resolution of 1.5–5 km globally and 350 m for selected areas (Bibring et al., 2005; Gendrin et al., 2005). Visible and near-infrared reflectance spectra are very sensitive to water and hydrated minerals.

In this paper, four gully-exposed sites at Terra Sirenum (36.5°S/198.2°E), the north of Reull Vallis (40.0°S/108.2°E), on the northeast wall of Hale Crater (35.5°S/324.6°E) and the upper Dao Vallis (33.1°S/93.2°E) (Fig. 1) were selected to investigate the presence of water, based on (1) availability of OMEGA images covering gully-exposed sites; (2) quality of the available OMEGA images; (3) compatible scale of the size of gully-exposed sites with the spatial resolution of the corresponding OMEGA image; (4) representation of different types of gully features located at relative lower latitudes for avoiding the effect of CO₂; and (5) appropriate Martian season and local time that OMEGA image of gully-exposed site was taken for avoiding the effect of water frost.

2. Methods

We analyzed reflectance spectra of OMEGA images, measured and compared the absorption band depths of water (molecular or

hydroxyl) on a pixel scale (statistically), and interpreted the abundances of water components in the surface soils and rocks at the gully-exposed sites (the target site) and its surrounding areas. The absorption depth of the water absorption bands is linearly proportional to the abundance of water-related materials by which the absorption is produced because absorption depth is proportional to the absorption intensity represented by the water absorption band (Clark and Roush, 1984). This is generally true for a small area where the environmental effects (mainly atmospheric abundance and composition, dust, and wind) are invariant and the effect of grain size is limited.

The OMEGA images downloaded from the European Space Agency (ESA) were first transformed to the tiff image format using the IDL code (SOFT03) developed by the ESA/OMEGA team. Atmospheric correction was conducted using the model provided by the ESA/OMEGA team. This model assumes that the Martian atmospheric column is homogeneous and the materials on the summit and at the base of Olympus Mons are identical. Atmospheric absorptions could be removed by dividing the reflectance spectra by a ratio of spectra acquired on Olympus Mons and scaled to the same column density of CO₂ (Langevin et al., 2005).

Reflectance spectra were extracted from a pixel or a group of pixels at the target site and from the surrounding pixel rings (as shown in Fig. 2). Reflectance spectra were also extracted pixel-by-pixel along cross sections through the target site in near E–W and N–S directions. The pixel(s) at the target site and five pixels away from the target site in both directions were investigated. This was assumed to be a reasonable range to observe the variation of the Martian surface materials around gully-exposed areas on the basis of the scale of a gully-exposed site (hundreds meters to a few kilometres) and a pixel in an OMEGA image (0.3–5 km). It is reasonable to assume that the centre of gully-exposed site might have been subjected to more frequent seepages of groundwater than the surroundings. So more water traces should have been left in the centre of gully-exposed site than the surroundings. A correlation coefficient between the absorption depths of water features and the distances from the centre outward is thus calculated and analyzed.

A continuum was removed to analyze absorption features as described by Clark (1981a) and Clark and Roush (1984). Continuum removal was employed to eliminate the influence of spectral background, which makes similar spectra distinctive and concentrates on the absorption features. The process can be expressed by

$$R_c(w) = R_a(w)/C(w) \quad (1)$$

where R_c is the continuum-removed observed spectrum; R_a is the apparent reflectance spectrum as a function of wavelength, and C is the continuum for the apparent spectrum.

In this paper, we focused our analysis on absorption features of wavelengths ranging from 0.97 to 2.55 μm with a total of 114 channels of OMEGA images. In this wavelength range, the presence of H₂O and/or OH can cause a number of absorptions. Water (H₂O) and hydroxyl (OH) in the state of a free molecule, and in minerals or organic matter generates distinct absorptions. The water molecule has three fundamental vibrations; ν_1 (symmetric OH stretch); ν_2 (H–O–H bend); and ν_3 (asymmetric OH stretch). The overtones of water (involving

Fig. 1. MOLA shaded relief images (left panel), MOC-NA images (middle panel), and OMEGA images (right panel) of the four investigated gully-exposed sites. MOLA images resolution is 0.015625 (1/64) by 0.015625 degrees. The white square in MOLA image denotes the gully location and matched point (red) in OMEGA image denotes the hydrated feature. (A) at 36.5°S/198.2°E, Terra Sirenum; (B) at 40.0°S, 108.2°E, the north of Reull Vallis; (C) at 35.5°S/324.6°E, the northeast wall of Hale Crater; and (D) at 33.1°S/93.2°E, the upper Dao Vallis. RGB composites of OMEGA images are 1.997 μm +1.529 μm +1.155 μm for A (orb1408_5), 1.997 μm +1.529 μm+1.084 μm for B (orb1887_3), 2.011 μm+1.529 μm+1.112 μm for C (orb1143_7), and 1.997 μm+1.529 μm+1.155 μm for D (orb1464_4). Scaled width of the MOC-NA images are 3.19 km for A (S0501463), 2.85 km for B (M0402479), 4.5 km for C (MOC2-1620-a), and 2.85 km for D (M1101601).

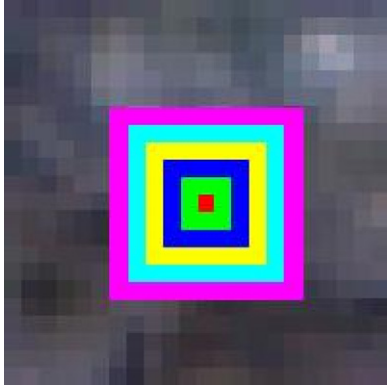


Fig. 2. Schematic location of a gully-exposed site as a pixel in the centre (red) and its surrounding areas as pixel rings in an OMEGA image. For example, the 1st ring (green) is a group of 8 pixels, the 2nd ring (blue) is a group of 16 pixels, the 3rd ring (yellow) is a group of 24 pixels, the 4th ring (cyan) is a group of 32 pixels, and the 5th ring (magenta) is a group of 40 pixels. (For interpretation of the references to colour in this figure legend, the reader is referred to the web version of this article.)

multiples of a single fundamental mode) and combinations (involving different modes of vibrations) were observed in reflectance spectra of the isolated water and the H₂O-bearing materials (Clark, 1999).

Isolated water molecules have absorption bands at 0.94 μm ($2\nu_1 + \nu_3$), 1.14 μm ($\nu_1 + \nu_2 + \nu_3$), 1.38 μm ($\nu_1 + \nu_3$), 1.45 μm ($2\nu_2 + \nu_3$), and $\sim 1.87\ \mu\text{m}$ ($\nu_2 + \nu_3$) (Hunt and Salisbury, 1970). Water in minerals has combination and overtone bands close to these positions (Clark et al., 1990). OH has only one stretching vibration (ν_{OH}) and its overtones are near 1.40 μm ($2\nu_{\text{OH}}$) and 0.95 μm ($3\nu_{\text{OH}}$) (e.g., Cloutis et al., 2006). For water ice, the overtones and combination bands are shifted to 1.04 (vs. 0.94) μm , 1.25 (vs. 1.13) μm , 1.50–1.66 (vs. 1.38–1.45) μm , and 1.96–2.05 (vs. 1.88) μm (e.g., Clark, 1981b; Cloutis et al., 2006). The combination of H–O–H and OH stretching and bending causes 1.80 μm (Cloutis et al., 2006) and 1.90 μm (Clark, 1999) absorption bands. The hydroxyl linked to metals produces a metal–OH bend. Combination vibrations involving the OH stretch and metal–O–H bend cause absorptions in the 2.00–2.50 μm range, such as 2.20 μm for AlOH and 2.29 μm for MgOH and FeOH (Clark et al., 1990).

The depths of absorption features of water vary as a function of water content and structure state (Dalton, 2003). The higher the abundance of a material is, the greater the corresponding absorption band depth. The absorption depth is calculated using two adjacent spectral channels of continuum spectra. The centre band of absorption can be expressed by

$$D = 1 - R_b/R_c \quad (2)$$

where D is the depth of absorption band; R_b is the reflectance at the band centre; and R_c is the reflectance of the continuum at the band centre.

A minimum noise fraction (MNF) transformation was used to separate the original bands into MNF bands of noise-free and MNF bands of noise, and then the inverse MNF was applied to convert the noise-free (less) MNF bands back into the original dimension using the first 20 bands. Therefore, absorption depths of water absorption bands were measured using ENVI software for an individual pixel or the mean of a pixel ring from continuum-removed reflectance spectra. Then we compared absorption band depths of the spectra at the target site and its surrounding areas, and pixel by pixel along a cross section through the target site.

3. Investigation of selected gully-exposed sites

3.1. Gully feature in Terra Sirenum (36.5°S/198.2°E)

Gullies were observed on the wall of an unnamed crater of about 3.8 km in diameter (36.5°S/198.2°E) in the MOC narrow-angle image S05-01463 with a spatial resolution of 1.56 m/pixel (Fig. 1A, middle panel). Among these gullies a light-toned flow about 300 m long was identified by Malin et al. (2006) on the northwest wall of the crater when they compared the MOC image taken in December 2001 ($L_s = 290^\circ$) and the image taken in April 2005 ($L_s = 193^\circ$). The light-toned flow was interpreted as a fresh deposit with liquid water seeping out onto the surface from a shallow aquifer (Malin et al. 2006).

The OMEGA image Orb1408_5 (Fig. 1A, right panel) was downloaded and processed based on the methods described above. The image was taken on February 21, 2005 ($L_s = 163.5^\circ$). The Mars local time of this site when the OMEGA image was taken was at about 11:05 am (MTC-11, Coordinated Mars Time) in the Martian southern hemisphere late winter. The pixel X: 106/Y: 139 (Lat. -36.477398 , Long. 198.218796E) in the image matches with the crater, where gullies were found. One pixel in the OMEGA image at the target site has the areal extent of about $3.9\ \text{km} \times 3.2\ \text{km}$ on the ground. This is about the same size as the crater itself.

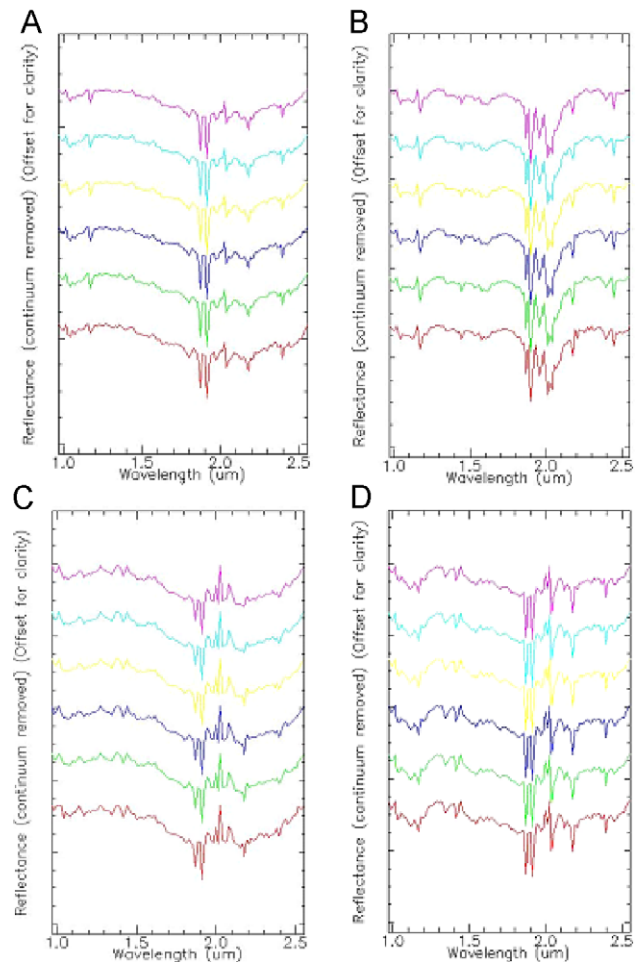


Fig. 3. Continuum-removed reflectance spectra of the target site and its surrounding pixel rings. From the bottom to the top are spectra of the target site (red), 1st pixel ring (green), 2nd pixel ring (blue), 3rd pixel ring (yellow), 4th pixel ring (cyan), and 5th pixel ring (magenta). (A) at Terra Sirenum, (B) at the north of Reull Vallis, (C) at the northeast wall of Hale Crater, (D) at the upper Dao Vallis. (For interpretation of the references to colour in this figure legend, the reader is referred to the web version of this article.)

Table 1
Data of absorption band depths of gully feature in Terra Sirenum (36.5°S/198.2°E).

| A. At the target site and its surrounding rings | | | | | | | | | | |
|--|---------------|---------------|---------------|---------------|---------------|---------------|---------------|---------------|---------------|---------------|
| Band range | 1.0121/1.0550 | 1.1555/1.1986 | 1.3568/1.4430 | 1.4861/1.5291 | 1.7291/1.8285 | 1.8285/1.8850 | 1.8850/1.9553 | 1.9553/2.0253 | 2.0253/2.0948 | 2.0948/2.2188 |
| Center | 1.0407 | 1.1699 | 1.3999 | 1.5004 | 1.8002 | 1.8709 | 1.9132 | 1.9693 | 2.0392 | 2.1776 |
| Target pixel | 0.017 | 0.021 | 0.007 | 0.003 | 0.019 | 0.07 | 0.09 | 0.019 | 0.045 | 0.036 |
| 1st | 0.014 | 0.027 | 0.007 | 0.002 | 0.016 | 0.071 | 0.089 | 0.02 | 0.04 | 0.032 |
| 2nd | 0.014 | 0.026 | 0.006 | 0.002 | 0.015 | 0.07 | 0.091 | 0.021 | 0.041 | 0.032 |
| 3rd | 0.013 | 0.025 | 0.006 | 0.002 | 0.016 | 0.067 | 0.092 | 0.02 | 0.041 | 0.032 |
| 4th | 0.013 | 0.025 | 0.005 | 0.002 | 0.018 | 0.068 | 0.09 | 0.019 | 0.039 | 0.036 |
| 5th | 0.013 | 0.026 | 0.005 | 0.002 | 0.016 | 0.071 | 0.089 | 0.02 | 0.039 | 0.035 |
| Correlation | 0.828 | -0.459 | 0.956 | 0.655 | 0.284 | 0.228 | 0.046 | -0.071 | 0.791 | -0.183 |
| B. In the cross section of East–West direction through the target site | | | | | | | | | | |
| East | 0.015 | 0.028 | 0.007 | 0.003 | 0.015 | 0.072 | 0.088 | 0.023 | 0.039 | 0.029 |
| | 0.016 | 0.024 | 0.008 | 0.002 | 0.02 | 0.073 | 0.091 | 0.018 | 0.037 | 0.033 |
| | 0.015 | 0.025 | 0.006 | 0.002 | 0.016 | 0.068 | 0.093 | 0.018 | 0.042 | 0.03 |
| | 0.017 | 0.024 | 0.008 | 0.003 | 0.021 | 0.066 | 0.097 | 0.023 | 0.044 | 0.03 |
| | 0.015 | 0.026 | 0.008 | 0.003 | 0.016 | 0.065 | 0.093 | 0.02 | 0.043 | 0.036 |
| Target | 0.017 | 0.021 | 0.007 | 0.003 | 0.019 | 0.07 | 0.09 | 0.019 | 0.045 | 0.036 |
| | 0.017 | 0.029 | 0.005 | 0.004 | 0.017 | 0.064 | 0.085 | 0.023 | 0.037 | 0.031 |
| | 0.016 | 0.032 | 0.008 | 0.002 | 0.016 | 0.081 | 0.087 | 0.021 | 0.04 | 0.033 |
| | 0.018 | 0.023 | 0.006 | 0.002 | 0.014 | 0.068 | 0.08 | 0.018 | 0.043 | 0.03 |
| | 0.019 | 0.025 | 0.007 | 0.002 | 0.014 | 0.071 | 0.087 | 0.021 | 0.036 | 0.03 |
| West | 0.017 | 0.028 | 0.009 | 0.003 | 0.015 | 0.067 | 0.089 | 0.027 | 0.043 | 0.03 |
| Correlation | -0.029 | -0.186 | -0.283 | 0.361 | 0.403 | -0.196 | 0.140 | -0.316 | 0.369 | 0.693 |
| C. In the cross section of South–North direction through the target site | | | | | | | | | | |
| South | 0.012 | 0.022 | 0.006 | 0.002 | 0.02 | 0.066 | 0.087 | 0.018 | 0.038 | 0.035 |
| | 0.011 | 0.02 | 0.005 | 0.002 | 0.023 | 0.071 | 0.089 | 0.02 | 0.043 | 0.036 |
| | 0.016 | 0.026 | 0.008 | 0.002 | 0.026 | 0.071 | 0.093 | 0.026 | 0.046 | 0.036 |
| | 0.018 | 0.023 | 0.006 | 0.003 | 0.021 | 0.074 | 0.091 | 0.024 | 0.044 | 0.034 |
| | 0.011 | 0.017 | 0.007 | 0.003 | 0.021 | 0.076 | 0.088 | 0.019 | 0.041 | 0.03 |
| Target | 0.017 | 0.021 | 0.007 | 0.003 | 0.019 | 0.07 | 0.09 | 0.019 | 0.045 | 0.036 |
| | 0.014 | 0.028 | 0.01 | 0.002 | 0.01 | 0.073 | 0.091 | 0.025 | 0.041 | 0.035 |
| | 0.016 | 0.021 | 0.006 | 0.002 | 0.012 | 0.069 | 0.093 | 0.025 | 0.041 | 0.022 |
| | 0.008 | 0.022 | 0.01 | 0.004 | 0.02 | 0.073 | 0.097 | 0.02 | 0.042 | 0.036 |
| | 0.019 | 0.021 | 0.004 | 0.005 | 0.021 | 0.076 | 0.098 | 0.022 | 0.039 | 0.042 |
| North | 0.012 | 0.023 | 0.008 | 0.004 | 0.012 | 0.082 | 0.098 | 0.02 | 0.038 | 0.042 |
| Correlation | 0.258 | -0.011 | 0.283 | -0.213 | -0.140 | -0.146 | -0.331 | 0.230 | 0.555 | -0.467 |

The target pixel and its five surrounding rings of pixels were selected as regions of interest (ROIs). Their reflectance spectra after MNF transformation are shown in Fig. 3A. The spectra of the target site and its surroundings are similar, which indicates that the materials at the target site and in its surrounding areas are similar. Ten absorption bands were observed and examined, among them the water-related bands at 1.04, 1.40, 1.50, 1.80, 1.87, 1.91, 2.04, and 2.18 μm . Absorption bands at 1.17 μm related to ferrous materials (coordinated by H_2O , Cloutis et al., 2006) and at 1.97 μm related to CO_2 ice (such as clathrate, CO_2 in water ice, Bernstein et al., 2005) were also examined. The absorption band centres, band ranges, and absorption band depths are shown in Table 1. The correlation coefficients between absorption band depths and the locations (reverse distance) of pixel rings relative to the target site were calculated (Table 1).

Table 1A indicates that in the target pixel the absorption depths of all water-related bands were larger or equal to those of its adjacent pixel rings except the atmospheric water vapour band (1.87 μm). The variations from the target pixel to the adjacent pixel rings were 21.4%, 50.0%, 18.8%, 11.2%, 12.5%, and 12.5%, for the 1.04, 1.50, 1.80, 1.91, 2.04, and 2.18 μm bands, respectively. The variations were 16.7% from the target pixel to the second pixel ring and 40% to the fourth pixel ring for the 1.40 μm band. At 1.04, 1.40, 1.50, and 2.04 μm the absorption depths decreased as the distances increased from the target site, with a correlation coefficient of 0.83, 0.97, 0.66, and 0.79, respectively (Fig. 4A). In contrast, the absorption depths of the two non-water absorption bands (1.17 and 1.97 μm) and atmospheric water vapour absorption band at 1.87 μm in the target pixel were less than those of the surrounding pixel rings. There was no significant correlation found between the target pixel and adjacent rings for those bands, meaning that the materials in the region are similar, except for the water signatures associated with the gully formation that were indicated at the site.

Table 1 (B and C) displays absorption depths of the above band centres along the two cross sections (approximately W–E and S–N) through the target site. Once again, the absorption band depths at the target site were greater than that at the adjacent pixels for most absorption bands associated with water. In contrast, the absorption depths at the target site for 1.17, 1.87, and 1.97 μm bands were lower than or equal to the adjacent pixels. The elevations may affect absorption band depths, but no relationship between the elevation and absorption band depths was recognized when examining the relationship between the elevation of the two cross sections (Fig. 5A and B) and the absorption depths of the water-related bands.

3.2. Gully feature to the north of Reull Vallis (40.0°S/108.2°E)

An apron with digitate flows was observed to the north of Reull Vallis at 40.0°S/108.2°E (Malin and Edgett, 2000a) among a cluster of gullies in the MOC narrow-angle image M04-02479 (Fig. 1B, middle panel). This MOC image was taken on August 22, 1999 ($L_s = 192.5^\circ$) with a spatial resolution of 2.79 m/pixel. About five subsidiary channels merge into one downslope forming a gully system of about 1 km in width and 2 km in length.

The OMEGA image orb1887_3 (Fig. 1B, right panel) was taken at about 4:49 pm (MTC+7) on July 05, 2005 ($L_s = 243.0^\circ$), in the Martian southern hemisphere late spring. The pixel X:73/Y:32 (Lat. -40.009499 , Long. 108.204300E) was assigned to be the gully-exposed site based on their matched coordinates. One pixel in the OMEGA image at the target site has the areal extent of about 1.6 km \times 2.1 km on the ground. This is about the size of the apron with digitate flows.

The target pixel and its five surrounding pixel rings were selected as the regions of interest. Their reflectance spectra after

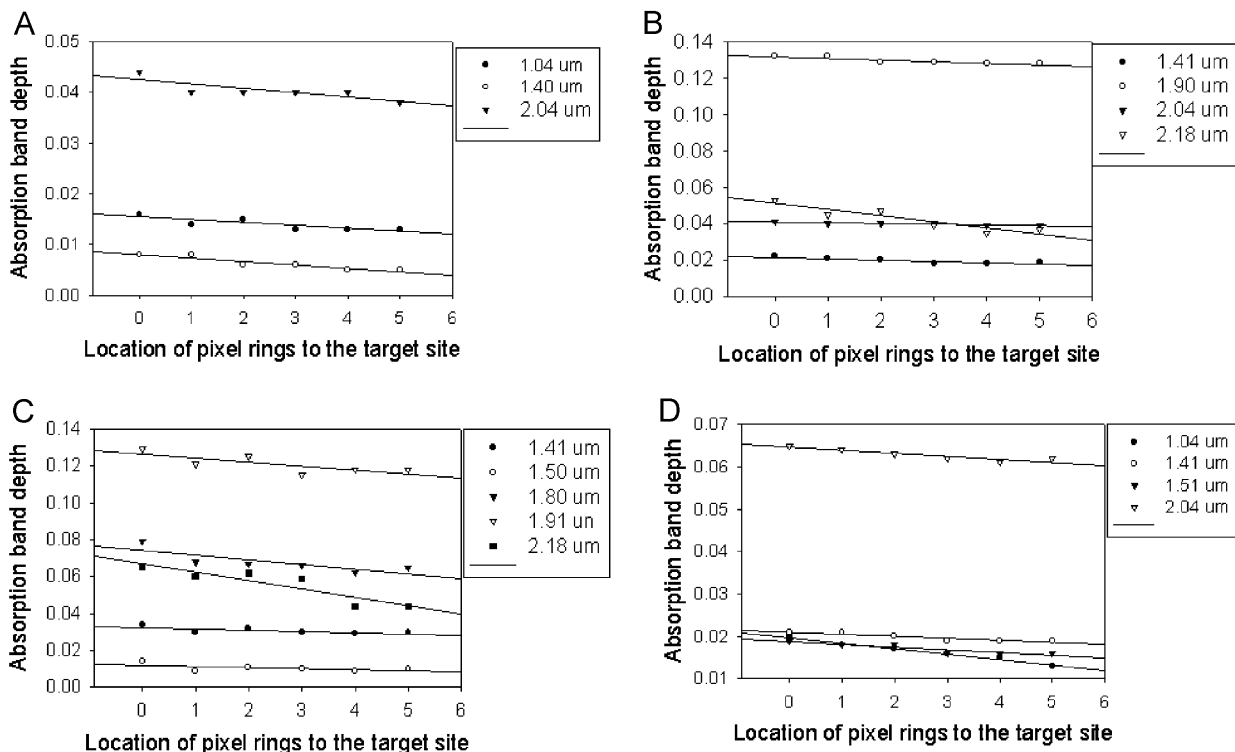


Fig. 4. The relationship of the absorption depths related to water and the location of pixel rings. The number 0 in X-axis represents the location of the target site, 1–5 corresponds to the 1st–5th ring from the target site. (A) at Terra Sirenum, (B) at the north of Reull Vallis, (C) at the northeast wall of Hale Crater, and (D) at the upper Dao Vallis.

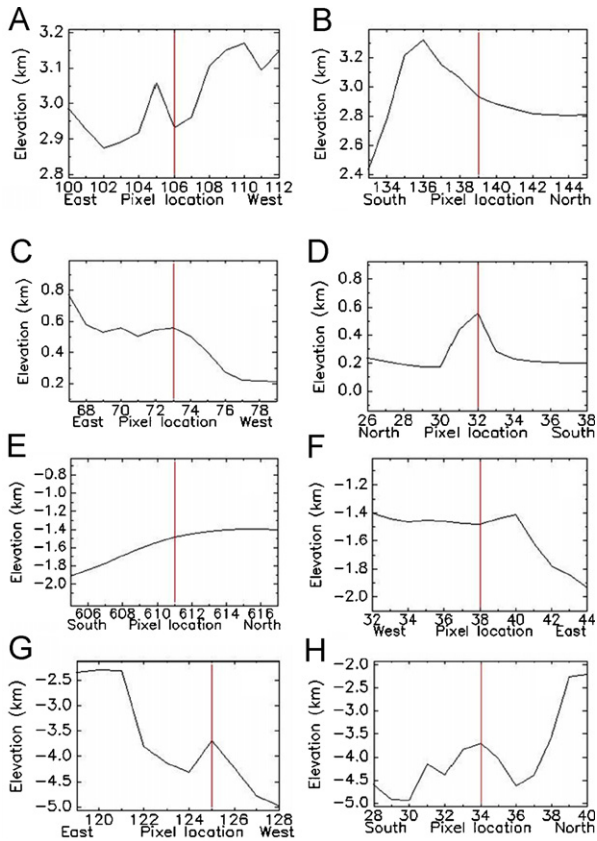


Fig. 5. Elevation profiles of the investigated sites. The vertical line is the location of the target pixel with each number representing spacing of pixels. A and B is at Terra Sirenum; C and D is at the north of Reull Vallis; E and F is at the northeast wall of Hale Crater; G and H is at the upper Dao Vallis.

MNF transformation are shown in Fig. 3B. Seven absorption bands were examined, including the water-related bands at 1.04, 1.41, 1.87, 1.90, 2.04, and 2.18 μm and the ferrous materials related one at 1.17 μm . In Table 2, the absorption band centres, band ranges, absorption band depths, and the correlation coefficients between absorption band depths and the locations (reverse distance) of pixel rings relative to the target site are shown.

As indicated in Table 2, the absorption depths of the target pixel are greater than or equal to those of the adjacent pixel ring for the water-related bands of 1.04, 1.41, 1.90, 2.04, and 2.18 μm , but reversely for the band of 1.17 μm and the water vapour-related bands of 1.87 μm . The decrease of absorption depths from the target site to the adjacent pixel ring were 5.8%, 4.8%, 2.5%, and 17.8% for the bands of 1.04, 1.41, 2.04, and 2.18 μm , respectively. Higher correlation coefficients (greater than 0.85) between these absorption depths and reverse distances to the target site were recognized for the bands of 1.41, 1.90, 2.04, and 2.18 μm (Fig. 4B). In contrast, the absorption depths of non-water absorption band (1.17 μm) and atmospheric water vapour absorption band at 1.87 μm in the target pixel were less than those of the surrounding pixel rings. The correlation coefficients for the two bands are also very low. The stronger signatures of water were only shown to be associated with the surface material at the gully-exposed site.

The absorption depths of the above bands along the two cross sections (approximately W–E and S–N) through the target site were also investigated. Once again, the absorption band depths at the target site were greater than or equal to that at the adjacent pixels for the absorption bands associated with water on the

ground rather than non-water and water vapour-related bands. Although no significant correlation between the water-related absorption depths and the reverse distance to the target site was found, no relationship between these absorption band depths and the change of elevation (Fig. 5C and D) was recognized.

3.3. Gully feature on the northeast wall of Hale Crater (35.5°S/324.6°E)

Several gullies with light-toned material on their floors and deposited in their aprons were observed on the northeast wall of Hale Crater (35.5°S/324.6°E) by the MOC team at Malin Space Science Systems (2000) (MOC2-1620-a is shown in Fig. 1C, middle panel). The light-toned deposits (about 1.5 km in length) may be produced by water flow during the past few years.

The matched OMEGA image orb1143_7 (Fig. 1C, right panel) was taken on December 8, 2004 ($L_s = 126.2$). The Mars local time when the OMEGA image was taken was at about 2:15 pm (MTC –2) in the Martian southern hemisphere middle winter. An individual pixel in the image at the site covers about 1.1 km \times 1.2 km area. The pixel X:38/Y:611 (Lat. –35.498600, Long. 324.592285) in the OMEGA image was assigned to be the target site due to their best match.

The reflectance spectra of the target site and five surrounding rings after the process of MNF transformation are shown in Fig. 3C. The absorptions of ten bands were examined, among them the water-related being 1.04, 1.41, 1.50, 1.80, 1.87, 1.91, 2.05, and 2.18 μm . As Table 3 indicated, the absorption depths of all water-related bands at the target site were greater than the adjacent pixel ring except the absorption of water vapour at 1.87 μm . The variations of absorption depths from the target site to the adjacent pixel ring is by 145.5%, 13.3%, 55.6%, 6.7%, 6.3%, and 8.3% for the bands of 1.04, 1.41, 1.50, 1.91, 2.05, and 2.18 μm . These variations are significantly greater than the variations of absorption depths from one pixel ring to another pixel ring for each absorption band above.

Some absorption bands show higher correlation between the absorption depths and the reverse distance to the target site but some do not. The absorption bands with the higher correlation coefficients are 1.41 μm (0.73), 1.50 μm (0.60), 1.80 μm (0.81), 1.91 μm (0.76), and 2.18 μm (0.90) (Fig. 4C). In contrast, non-water-related absorption bands at 1.17 and 1.97 μm displays negative correlation between the absorption depths and the reverse distance to the target site.

Through examination of the two cross sections passing through the gully-exposed site in the W–E and the N–S directions (Table 3), the absorption depths at the target site are higher or equal to that of the adjacent pixels for the most water-related bands. But most of these bands do not show a significant correlation between the absorption depths and the distance to the target site. No relationship was recognized between the variations of these absorption depths and the profiles of in-situ change of elevation in both the W–E and N–S directions (Fig. 5E and F).

3.4. Gully feature in the upper Dao Vallis (33.1°S/93.2°E)

Alcoves filled or partially filled with deposit materials at the site at 33.1°S/93.2°E were interpreted to be the result of sapping due to groundwater seeping out from subsurface layers (Malin and Edgett, 2000a). The features are common throughout the wall of Dao Vallis. The specific site is shown in the MOC narrow-angle image M11-01601 with spatial resolution of 2.78 m/pixel (Fig. 1D, middle panel).

Table 2
Data of absorption band depths of gully feature to the north of Reull Vallis (40.0°S/108.2°E).

| A. At the target site and its surrounding rings | | | | | | | | | |
|--|---------------|---------------|---------------|---------------|---------------|---------------|---------------|---------------|---------------|
| Band range | 1.0121/1.0550 | 1.1555/1.2849 | 1.3999/1.4717 | 1.8568/1.8850 | 1.8850/1.9272 | 1.9272/1.9834 | 1.9834/2.0253 | 2.0253/2.0531 | 2.1501/2.1914 |
| Center | 1.0407 | 1.1699 | 1.4130 | 1.8709 | 1.8991 | 1.9553 | 2.0113 | 2.0392 | 2.1776 |
| Target | 0.018 | 0.053 | 0.022 | 0.07 | 0.132 | 0.065 | 0.057 | 0.041 | 0.053 |
| 1st ring | 0.017 | 0.054 | 0.021 | 0.079 | 0.132 | 0.065 | 0.053 | 0.04 | 0.045 |
| 2nd ring | 0.018 | 0.051 | 0.02 | 0.074 | 0.129 | 0.065 | 0.053 | 0.04 | 0.047 |
| 3rd ring | 0.019 | 0.052 | 0.018 | 0.077 | 0.129 | 0.062 | 0.052 | 0.04 | 0.039 |
| 4th ring | 0.018 | 0.053 | 0.018 | 0.074 | 0.128 | 0.061 | 0.053 | 0.039 | 0.035 |
| 5th ring | 0.018 | 0.052 | 0.019 | 0.072 | 0.128 | 0.063 | 0.053 | 0.039 | 0.037 |
| Correlation | −0.338 | 0.357 | 0.851 | 0.033 | 0.919 | 0.759 | 0.638 | 0.923 | 0.919 |
| B. In the cross section of East–West direction through the target site | | | | | | | | | |
| East | 0.02 | 0.057 | 0.017 | 0.072 | 0.035 | 0.068 | 0.074 | 0.041 | 0.044 |
| | 0.017 | 0.059 | 0.02 | 0.071 | 0.128 | 0.071 | 0.059 | 0.04 | 0.049 |
| | 0.018 | 0.063 | 0.018 | 0.068 | 0.129 | 0.057 | 0.055 | 0.041 | 0.053 |
| | 0.022 | 0.067 | 0.018 | 0.069 | 0.129 | 0.06 | 0.05 | 0.042 | 0.04 |
| | 0.02 | 0.059 | 0.021 | 0.07 | 0.132 | 0.064 | 0.055 | 0.04 | 0.039 |
| Target | 0.018 | 0.053 | 0.022 | 0.07 | 0.132 | 0.065 | 0.057 | 0.041 | 0.053 |
| | 0.02 | 0.051 | 0.022 | 0.072 | 0.13 | 0.07 | 0.043 | 0.041 | 0.032 |
| | 0.022 | 0.05 | 0.021 | 0.08 | 0.131 | 0.069 | 0.057 | 0.04 | 0.039 |
| | 0.022 | 0.049 | 0.019 | 0.074 | 0.13 | 0.068 | 0.053 | 0.04 | 0.042 |
| | 0.018 | 0.056 | 0.019 | 0.073 | 0.129 | 0.061 | 0.056 | 0.041 | 0.054 |
| West | 0.016 | 0.06 | 0.018 | 0.081 | 0.127 | 0.063 | 0.057 | 0.04 | 0.045 |
| Correlation | 0.364 | −0.245 | 0.794 | −0.355 | 0.491 | 0.036 | −0.569 | 0.185 | −0.292 |
| C. In the cross section of South–North direction through the target site | | | | | | | | | |
| North | 0.016 | 0.055 | 0.022 | 0.066 | 0.132 | 0.068 | 0.053 | 0.034 | 0.008 |
| | 0.022 | 0.043 | 0.02 | 0.071 | 0.128 | 0.07 | 0.05 | 0.039 | 0.017 |
| | 0.023 | 0.055 | 0.019 | 0.069 | 0.13 | 0.066 | 0.052 | 0.039 | 0.009 |
| | 0.018 | 0.053 | 0.022 | 0.071 | 0.121 | 0.061 | 0.047 | 0.039 | 0.057 |
| | 0.015 | 0.053 | 0.022 | 0.075 | 0.133 | 0.062 | 0.054 | 0.037 | 0.045 |
| Target | 0.018 | 0.053 | 0.022 | 0.07 | 0.132 | 0.065 | 0.057 | 0.041 | 0.053 |
| | 0.021 | 0.054 | 0.023 | 0.097 | 0.13 | 0.071 | 0.052 | 0.04 | 0.04 |
| | 0.02 | 0.051 | 0.021 | 0.074 | 0.131 | 0.067 | 0.059 | 0.04 | 0.036 |
| | 0.019 | 0.065 | 0.022 | 0.078 | 0.131 | 0.056 | 0.044 | 0.04 | 0.068 |
| | 0.015 | 0.057 | 0.018 | 0.067 | 0.126 | 0.061 | 0.053 | 0.04 | 0.046 |
| South | 0.019 | 0.043 | 0.027 | 0.07 | 0.129 | 0.061 | 0.05 | 0.039 | 0.068 |
| Correlation | 0.018 | 0.217 | −0.049 | 0.478 | 0.173 | 0.090 | 0.344 | 0.443 | 0.236 |

The OMEGA image orb1464_4 (Fig. 1D, right panel) processed was taken on March 3, 2005 ($L_s = 168.9$). The Mars local time at the OMEGA image acquisition was at about 10:26 am (MTC+6) in the Martian southern hemisphere late winter. One pixel at the site was about $3.9 \text{ km} \times 3.3 \text{ km}$. The ROI of four pixels X: 125–126/Y:33–34 (Lat. -33.068600 to -33.120399 , Long. 93.183800 – 93.257896E) was selected to match up with the site exposing alcoves and associated deposits.

The absorptions of ten bands after MNF transformation were examined (Fig. 3D). The absorption depths of water-related bands (1.04, 1.41, 1.51, 1.91, 2.04, and $2.18 \mu\text{m}$) at the target site were greater than or equal to those in the adjacent pixel ring (Table 4A). The variations from the target site to the adjacent pixel rings are 5.6%, 5.6%, 2.9%, 3.1%, and 14.7% for the absorption bands of 1.04, 1.41, 1.51, 1.91, 2.04, and $2.18 \mu\text{m}$. In contrast, the absorption depths of non-water-related bands (1.17, 1.34, and $1.97 \mu\text{m}$) and water vapour-related band ($1.87 \mu\text{m}$) are smaller at the target site than the adjacent pixel ring.

The absorption depths of the 1.04, 1.41, 1.51, and $2.04 \mu\text{m}$ bands showed spatial variations with high-correlation coefficients (above 0.92) (Fig. 4D). In contrast, the $1.87 \mu\text{m}$ band (atmospheric H_2O) showed a reverse trend and the 1.17 and $1.34 \mu\text{m}$ (non-water absorption bands) remained fairly stable. The inconsistency of absorption depths of these bands might indicate that the stronger absorptions of 1.04, 1.41, 1.54, and $2.04 \mu\text{m}$ at the target site compared to the surrounding areas have to be attributed to the influences of water components in the rocks and soil, but not the atmosphere or systematic errors of instruments and analysis.

Along the cross sections (Table 4B and C), the absorption depths related to water essentially showed an increasing trend towards the south in the N–S direction and towards the west in

the E–W direction. The trends are likely attributed to the profile of landforms at the site (Fig. 5G and F), because the differences of elevation were about 2.8 km between both ends of the N–S cross section and 2.7 km between both ends of the E–W cross section. The significant difference of elevation led to the accumulation of water in the lowland areas. Nevertheless, the absorption depths at the target site were still larger than their adjacent pixels for most of the water absorption bands.

4. Discussion

Investigation of the four sites in this study showed greater absorption depths of water-related bands at the gully-exposed sites than those at the adjacent pixel ring, and smaller absorption depths of water-related bands in the surrounding pixel rings. The decreasing trend of some absorption depths when moving further away from the site was also observed at the investigated gully-exposed sites. This likely indicates higher abundance of water ice, OH-bearing or hydrated materials in surface soil at the gully-exposed sites.

Absorptions of the investigated sites commonly occurred at all or part of bands, ~ 1.04 , ~ 1.17 , ~ 1.34 , ~ 1.40 , ~ 1.50 , ~ 1.80 – 1.87 , ~ 1.91 , ~ 1.97 , ~ 2.04 , and $\sim 2.18 \mu\text{m}$, although a few other weak absorptions were recognized occasionally. Recognizable were the shifts of band positions, and the variation of absorption shapes, width (full width at half maximum) and depth of band centre from pixel to pixel in most cases. Analyzing absorption features of reflectance spectra and measuring their depths are vital to studying subtle differences of composition and structure of materials.

Table 3

Data of absorption band depths of gully feature on the northeast wall of Hale Crater (35.5°S/324.6°E).

| A. At the target site and its surrounding rings | | | | | | | | | | |
|--|---------------|---------------|---------------|---------------|---------------|---------------|---------------|---------------|---------------|---------------|
| Band range | 1.0121/1.0550 | 1.1555/1.1986 | 1.3855/1.4430 | 1.4861/1.5291 | 1.7291/1.8285 | 1.8285/1.8850 | 1.8850/1.9413 | 1.9413/1.9973 | 2.0253/2.0809 | 2.0948/2.2188 |
| Center | 1.0407 | 1.1699 | 1.4143 | 1.5004 | 1.8002 | 1.8709 | 1.9132 | 1.9693 | 2.0531 | 2.1776 |
| Target pixel | 0.026 | 0.013 | 0.034 | 0.014 | 0.079 | 0.011 | 0.129 | 0.041 | 0.085 | 0.065 |
| 1st | 0.011 | 0.009 | 0.03 | 0.009 | 0.068 | 0.019 | 0.121 | 0.04 | 0.08 | 0.06 |
| 2nd | 0.015 | 0.011 | 0.032 | 0.011 | 0.067 | 0.019 | 0.125 | 0.041 | 0.082 | 0.062 |
| 3rd | 0.015 | 0.012 | 0.03 | 0.01 | 0.066 | 0.014 | 0.115 | 0.04 | 0.085 | 0.059 |
| 4th | 0.015 | 0.015 | 0.029 | 0.009 | 0.062 | 0.016 | 0.118 | 0.044 | 0.081 | 0.044 |
| 5th | 0.016 | 0.013 | 0.03 | 0.01 | 0.065 | 0.015 | 0.118 | 0.043 | 0.086 | 0.044 |
| Correlation | 0.471 | -0.498 | 0.728 | 0.600 | 0.814 | -0.104 | 0.764 | -0.683 | -0.237 | 0.900 |
| B. In the cross section of East–West direction through the target site | | | | | | | | | | |
| East | 0.022 | 0.005 | 0.03 | 0.011 | 0.066 | 0.028 | 0.116 | 0.037 | 0.075 | 0.073 |
| | 0.021 | 0.029 | 0.024 | 0.009 | 0.061 | 0.02 | 0.107 | 0.049 | 0.078 | 0.052 |
| | 0.023 | 0.012 | 0.029 | 0.011 | 0.066 | 0.01 | 0.117 | 0.051 | 0.091 | 0.059 |
| | 0.034 | 0.029 | 0.029 | 0.011 | 0.067 | 0.014 | 0.12 | 0.044 | 0.085 | 0.057 |
| | 0.009 | 0.003 | 0.03 | 0.012 | 0.072 | 0.018 | 0.123 | 0.042 | 0.077 | 0.055 |
| Target | 0.026 | 0.016 | 0.034 | 0.014 | 0.079 | 0.011 | 0.129 | 0.041 | 0.085 | 0.056 |
| | 0.025 | 0.006 | 0.031 | 0.012 | 0.071 | 0.01 | 0.129 | 0.035 | 0.082 | 0.054 |
| | 0.02 | 0.015 | 0.032 | 0.014 | 0.065 | 0.016 | 0.129 | 0.052 | 0.085 | 0.063 |
| | 0.014 | 0.015 | 0.032 | 0.011 | 0.051 | 0.009 | 0.113 | 0.043 | 0.082 | 0.063 |
| | 0.011 | 0.017 | 0.032 | 0.01 | 0.061 | 0.01 | 0.115 | 0.044 | 0.081 | 0.062 |
| West | 0.012 | 0.011 | 0.033 | 0.01 | 0.057 | 0.019 | 0.128 | 0.048 | 0.084 | 0.05 |
| Correlation | 0.321 | -0.077 | 0.251 | 0.757 | 0.718 | -0.505 | 0.534 | -0.246 | 0.254 | -0.273 |
| C. In the cross section of South–North direction through the target site | | | | | | | | | | |
| South | 0.014 | 0.026 | 0.031 | 0.009 | 0.073 | 0.022 | 0.119 | 0.026 | 0.097 | 0.07 |
| | 0.018 | 0.024 | 0.032 | 0.015 | 0.054 | 0.01 | 0.116 | 0.047 | 0.089 | 0.093 |
| | 0.023 | 0.025 | 0.033 | 0.006 | 0.074 | 0.026 | 0.115 | 0.025 | 0.097 | 0.079 |
| | 0.009 | 0.024 | 0.042 | 0.016 | 0.06 | 0.034 | 0.137 | 0.015 | 0.096 | 0.069 |
| | 0.016 | 0.009 | 0.028 | 0.005 | 0.08 | 0.02 | 0.109 | 0.043 | 0.085 | 0.075 |
| Target | 0.026 | 0.019 | 0.034 | 0.014 | 0.079 | 0.011 | 0.129 | 0.041 | 0.085 | 0.065 |
| | 0.019 | 0.008 | 0.025 | 0.009 | 0.079 | 0.016 | 0.138 | 0.038 | 0.081 | 0.052 |
| | 0.03 | 0.008 | 0.031 | 0.011 | 0.074 | 0.019 | 0.125 | 0.045 | 0.079 | 0.076 |
| | 0.045 | 0.015 | 0.028 | 0.012 | 0.069 | 0.014 | 0.125 | 0.05 | 0.084 | 0.052 |
| | 0.013 | 0.015 | 0.03 | 0.01 | 0.066 | 0.015 | 0.136 | 0.037 | 0.077 | 0.078 |
| North | 0.026 | 0.016 | 0.031 | 0.011 | 0.065 | 0.013 | 0.115 | 0.035 | 0.077 | 0.054 |
| Correlation | 0.064 | -0.442 | 0.012 | -0.003 | 0.585 | 0.071 | 0.302 | 0.164 | -0.079 | -0.153 |

The overtones and combinations of vibrations of water at ~ 1.40 and $\sim 1.91 \mu\text{m}$, the lower frequencies of water ice at ~ 1.50 and $\sim 2.04 \mu\text{m}$, and the combination of metal–OH bend and OH stretch at 2.18, etc. were evident for most reflectance spectra of OMEGA images at gully-exposed sites on Mars. In addition, the following was observed: a weak absorption of water ice at $1.04 \mu\text{m}$; absorption at $1.80 \mu\text{m}$ attributed to a combination of H–O–H and OH stretching and bending (Cloutis et al., 2006); and absorption of atmospheric water at $1.87 \mu\text{m}$. If the investigated site is close to the polar areas, the absorptions of CO_2 ice might dominate reflectance spectra and severely affect the measurement of subtle variation of water-related absorptions.

The absorption band at $1.91 \mu\text{m}$ was the most obvious among the absorptions of water-related bands and its depth was 3% or greater at the target sites than the adjacent areas for four investigated sites. The absorption depths at $1.80 \mu\text{m}$ were about 16% greater at the target site than the adjacent area at two sites (Terra Sirenum, $36.5^\circ\text{S}/198.2^\circ\text{E}$ and the northeast wall of Hale Crater, $35.5^\circ\text{S}/324.6^\circ\text{E}$) and showed a higher correlation (0.814) with respect to the target site at the gully-exposed site of the northeast wall of Hale Crater. Absorption at $1.80 \mu\text{m}$ is not significantly overlapped by bands from other common minerals (Cloutis et al., 2006). The absorptions at the $1.41 \mu\text{m}$ band were not significant in regard to absolute depths, but they were the largest at the target sites rather than in the surrounding areas. Higher correlation (greater than 0.83) between the absorption depth of $1.41 \mu\text{m}$ and the reverse distance to the target site was shown at two gully-exposed sites (Terra Sirenum, and the upper Dao Vallis, $33.1^\circ\text{S}/93.2^\circ\text{E}$).

The absorption depths of water ice at the 1.04 , 1.50 and $2.04 \mu\text{m}$ bands were all greater at the target sites than those at

adjacent pixel rings. The largest variations of absorption depths from the target site to the adjacent ring was 136% for $1.04 \mu\text{m}$ and 56% for $1.50 \mu\text{m}$ at the northeast wall of Hale Crater, and 13% for $2.04 \mu\text{m}$ at the site of Terra Sirenum. Higher correlation coefficients between the absorption depths of these bands and the reverse distance to the target site were recognized at two sites (Terra Sirenum and the upper Dao Vallis). The absorption of $1.50 \mu\text{m}$ is thought to be the best band to monitor water ice on the Martian surface with OMEGA image (Langevin et al., 2007).

The absorption depths at $2.18 \mu\text{m}$ were all the greatest at the target sites and were about 8.3–17.8% greater than those at adjacent pixel rings for the four investigated sites. High-correlation coefficients (> 0.9) between the absorption depths and the reverse distance to the target site were recognized at two gully-exposed sites (the north of Reull Vallis, $40.0^\circ\text{S}/108.2^\circ\text{E}$ and the northeast wall of Hale Crater). The absorption is associated with metal–OH bonds, but S–O bonding incorporated with hydroxyl may play a role.

Absorption depths of the water-related bands had a maximum at the target sites, even given that their variations were affected by extreme changes of the elevation. In some cross sections, the variations of absorption depths were consistent with the extensions of the gully-exposed sites. This is likely the reason that the correlations between water-related absorption depths and reverse distance from the target sites present negative values in some cross sections.

In contrast, non-water-associated absorption bands such as those less than $1.20 \mu\text{m}$, at $1.97 \mu\text{m}$, and water vapour absorption ($1.87 \mu\text{m}$) usually did not show the same characteristics as water-related absorption bands. The absorption depths of these bands were less at the target site than the adjacent pixel rings at all the

Table 4
Data of absorption band depths of gully feature in the upper Dao Vallis (33.1°S/93.2°E).

| A. At the target site and its surrounding rings | | | | | | | | | | |
|---|---------------|----------------|---------------|---------------|---------------|---------------|---------------|---------------|---------------|---------------|
| Band range | 1.0121/1.0550 | 1.01411/1.1842 | 1.3136/1.3855 | 1.3855/1.4430 | 1.4430/1.6150 | 1.8586/1.8850 | 1.8850/1.9413 | 1.9413/1.9973 | 2.0253/2.0948 | 2.1363/2.1914 |
| Centre | 1.040 | 1.17 | 1.342 | 1.414 | 1.514 | 1.871 | 1.913 | 1.969 | 2.039 | 2.178 |
| Target | 0.019 | 0.018 | 0.013 | 0.021 | 0.019 | 0.06 | 0.07 | 0.020 | 0.066 | 0.039 |
| 1st ring | 0.018 | 0.020 | 0.014 | 0.021 | 0.018 | 0.061 | 0.068 | 0.022 | 0.064 | 0.034 |
| 2nd ring | 0.017 | 0.020 | 0.015 | 0.02 | 0.018 | 0.06 | 0.07 | 0.023 | 0.064 | 0.038 |
| 3rd ring | 0.016 | 0.019 | 0.015 | 0.019 | 0.016 | 0.061 | 0.07 | 0.017 | 0.064 | 0.038 |
| 4th ring | 0.015 | 0.019 | 0.014 | 0.019 | 0.016 | 0.061 | 0.07 | 0.014 | 0.062 | 0.036 |
| 5th ring | 0.014 | 0.018 | 0.014 | 0.019 | 0.016 | 0.061 | 0.068 | 0.019 | 0.062 | 0.038 |
| Correlation | 1.000 | 0.239 | −0.355 | 0.924 | 0.925 | −0.621 | 0.207 | 0.565 | 0.923 | 0.262 |
| B. In the cross section of South–West direction through the target site | | | | | | | | | | |
| South | 0.015 | 0.024 | 0.024 | 0.024 | 0.023 | 0.064 | 0.073 | 0.032 | 0.068 | 0.031 |
| | 0.021 | 0.023 | 0.024 | 0.022 | 0.02 | 0.057 | 0.073 | 0.028 | 0.068 | 0.033 |
| | 0.022 | 0.022 | 0.019 | 0.022 | 0.021 | 0.059 | 0.075 | 0.024 | 0.071 | 0.030 |
| | 0.016 | 0.021 | 0.017 | 0.022 | 0.021 | 0.062 | 0.074 | 0.027 | 0.07 | 0.036 |
| | 0.016 | 0.022 | 0.017 | 0.024 | 0.021 | 0.06 | 0.067 | 0.024 | 0.067 | 0.034 |
| Target | 0.027 | 0.017 | 0.015 | 0.022 | 0.021 | 0.059 | 0.07 | 0.018 | 0.067 | 0.033 |
| Target | 0.025 | 0.019 | 0.015 | 0.02 | 0.019 | 0.065 | 0.072 | 0.021 | 0.065 | 0.044 |
| | 0.017 | 0.023 | 0.014 | 0.019 | 0.017 | 0.062 | 0.068 | 0.020 | 0.061 | 0.040 |
| | 0.015 | 0.018 | 0.012 | 0.019 | 0.016 | 0.059 | 0.07 | 0.017 | 0.06 | 0.045 |
| | 0.014 | 0.020 | 0.013 | 0.019 | 0.016 | 0.061 | 0.066 | 0.020 | 0.06 | 0.043 |
| | 0.015 | 0.020 | 0.013 | 0.018 | 0.015 | 0.06 | 0.07 | 0.018 | 0.057 | 0.035 |
| North | 0.014 | 0.019 | 0.012 | 0.017 | 0.014 | 0.061 | 0.068 | 0.013 | 0.061 | 0.039 |
| Correlation | 0.572 | −0.373 | −0.309 | 0.154 | 0.209 | 0.124 | −0.140 | −0.171 | 0.128 | 0.301 |
| C. In the cross section of East–West direction through the target site | | | | | | | | | | |
| East | 0.018 | 0.015 | 0.011 | 0.017 | 0.013 | 0.059 | 0.068 | 0.019 | 0.059 | 0.043 |
| | 0.014 | 0.014 | 0.012 | 0.018 | 0.014 | 0.058 | 0.068 | 0.018 | 0.061 | 0.046 |
| | 0.016 | 0.016 | 0.012 | 0.018 | 0.014 | 0.06 | 0.07 | 0.014 | 0.061 | 0.047 |
| | 0.018 | 0.021 | 0.012 | 0.018 | 0.014 | 0.062 | 0.069 | 0.017 | 0.06 | 0.048 |
| | 0.017 | 0.017 | 0.013 | 0.018 | 0.015 | 0.058 | 0.067 | 0.020 | 0.059 | 0.047 |
| Target | 0.025 | 0.019 | 0.013 | 0.019 | 0.017 | 0.058 | 0.069 | 0.021 | 0.061 | 0.044 |
| Target | 0.014 | 0.020 | 0.015 | 0.02 | 0.019 | 0.065 | 0.072 | 0.019 | 0.065 | 0.042 |
| | 0.020 | 0.021 | 0.016 | 0.021 | 0.02 | 0.063 | 0.072 | 0.023 | 0.068 | 0.041 |
| | 0.019 | 0.023 | 0.02 | 0.021 | 0.02 | 0.061 | 0.075 | 0.027 | 0.068 | 0.030 |
| Correlation | 0.364 | 0.631 | 0.410 | 0.600 | 0.666 | 0.403 | 0.311 | 0.312 | 0.380 | −0.105 |

investigated sites except for the site at the northeast wall of Hale Crater. Some of them even showed a reverse relation to water-related bands, that is, the absorption depths increased with distance from the target site. Absorptions at a wavelength of less than the 1.20 μm band are usually associated with transition elements, most commonly ferric and ferrous minerals. They may be caused by iron atoms linking through shared oxygen or hydroxyl ions (Rossman, 1975), and ferrous crystal field transition or coordination with H_2O and SO_4^{2-} (Cloutis et al., 2006). The absorption at 1.97 μm is the contribution of CO_2 ice (e.g., Bernstein et al., 2005), which is detected at the four investigated sites. Atmospheric water vapour at 1.87 μm did not follow the trend of absorption depths as other forms of water in the surface soil.

For a small local area in the same OMEGA image, the environmental and instrumental conditions should be the same when these pixels were imaged. They were also subjected to the same image processing procedure including atmospheric correction. Thus, the greater absorption band depths indicated a higher content of water in the surface materials at the target sites than their surrounding areas.

The stronger signatures of water at the gully-exposed sites may be caused by water ice, isolated water molecules or hydroxyl groups in the soils, or seasonal water frost on the surface (Svitek and Murray, 1990; Reiss and Jaumann, 2003; Schorghofer and Edgett, 2006; Bellucci et al., 2007). Water frost was not likely the main cause because the images we investigated were taken in the Martian spring, in the Martian late winter, or in the early afternoon of Mars local time in the middle of winter. The observed frost appears during the period of early to mid southern hemisphere winter but not in late winter and spring times (Schorghofer and Edgett, 2006). So at least three of the four investigated OMEGA images were not taken in a season in which water frost would be expected. Even for the image taken in the middle of winter, the local surface temperature could be higher than 200 K (the sublimation point of water frost) at about 2:15 pm of the Martian day. But the effect of water frost on the absorption depths of water-related bands at gully-exposed sites deserves scrutiny, especially for the image taken in the middle winter time.

The pressure–temperature conditions on the surface of Mars are very close to the triple point of water, thus some water will likely freeze very fast in the loose materials. Alternatively, it may stay attached to the mineral surface or evaporate into the atmosphere after it has seeped out from the subsurface. Alteration could take place if hydrothermal fluids were involved and remained there for a fairly long period of time. So the accumulation of water at the gully-exposed sites implies that liquid water was once likely more active at the site than in its surrounding regions. Subsequently, liquid water was involved in the formation of the gully features and associated deposits.

The extension of about 5 pixels away from the target site was considered to be a reasonable range for the investigation, because the size of gully-exposed sites is about the size of an individual pixel (1.5–5 \times 1.5–5 km^2) in the OMEGA image. The influence of the residual of atmospheric correction or the systematic errors of the imaging spectrometer on the absorptions of reflectance spectra should be limited because (1) all absorption band depths at a specific site were calculated in the same OMEGA image, so all pixels were subject to the same processes; (2) the analysis of absorption variations were restricted in scope to a few pixels, which were imaged almost at the same time, with the same atmospheric conditions and under the same solar radiation; and (3) the trace content (0.03%) of water vapour in the Martian atmosphere does not make much difference in regard to absorption band depths (a few to tens percent) within the elevation change of the landform in hundreds of meters.

There are a variety of factors that may limit the conclusions drawn from this study. They include: (1) limited knowledge of grain size that might have affected the absorption depth; (2) the influence of seasonal temperature changes on imaged materials; (3) strong CO_2 absorption features at wavelengths around 2 μm both in the solid state and in the atmosphere (Langevin et al. 2007), especially for the gully-exposed site close to the polar areas; (4) the limitation of the spatial resolution of OMEGA hyperspectral images in the case study; and (5) errors in registering gully-exposed sites found from MOC images to OMEGA images due to the possible inaccuracy of two geo-referencing systems.

Certainly care has to be exercised in the interpretation of absorption-related water data. For example, no hydrated mineral was detected at the gully-exposed site in the Centauri Montes region in the hyperspectral image taken by the Compact Reconnaissance Imaging Spectrometer for Mars (CRISM) (McEwen et al., 2007), where light-toned deposits were thought to be the fresh deposits due to liquid water flow (Malin et al., 2006). Instead, numerical flow modelling showed that the deposits are more consistent with dry landslides. However, gully formation due to liquid water agent could not be ruled out (Pelletier et al., 2008).

Nevertheless, in this study we found a clear trend of variation of water-related absorption depths between gullies and their surrounding areas at our investigated gully-exposed sites. More analysis of hyperspectral image at higher spatial resolution such as CRISM (when they become available) should be done to further examine the conclusions put forward here.

5. Conclusions

The depth of the water-related absorption bands was observed to be greater at gully-exposed site than in their surrounding areas, thus supporting the conclusion that the formation of gullies has involved processes associated with liquid water. Subtle variations of absorption band depths, especially their trends provide insights in identifying small differences of materials with very similar reflectance spectra due to the sensitivity of imaging spectroscopy of material composition and structure. Further study of hyperspectral images is desirable with higher spatial and spectral resolutions (e.g., CRISM) for the better understanding of the water occurrence at gully sites.

Acknowledgements

We are indebted to the ESA/OMEGA team for making available OMEGA hyperspectral images to us and providing algorithm for atmospheric correction. We also like to thank the MGS/MOC team for making available MOC high-resolution images. We especially thank Dr. John A. Wolff, Dr. Joan Wu and two anonymous reviewers for their critical and insightful comments which help to improve the paper significantly. Author Xie acknowledges the funding support from the NASA/Texas Space Grant Consortium New Investigations Program (#NNG05GE96 H).

References

- Arvidson, R.E., Poulet, F., Bibring, J.-P., Wolff, M., Gendrin, A., Morris, R.V., Freeman, J.J., Langevin, Y., Mangold, N., Bellucci, G., 2005. Spectral reflectance and morphologic correlations in eastern Terra Meridiani, Mars. *Science* 307, 1591–1594.
- Bart, G.D., 2007. Comparison of small lunar landslides and Martian gullies. *Icarus* 187 (2), 417–421.
- Bellucci, G., et al., 2007. Evidence for enhanced hydration on the northern flank of Olympus Mons, Mars. *Icarus* 192, 361–377.

- Bernstein, M.P., Cruikshank, D.P., Sandford, S.A., 2005. Near-infrared laboratory spectra of solid H₂O/CO₂ and CH₃OH/CO₂ ice mixtures. *Icarus* 179, 527–534.
- Bibring, J.-P., Langevin, Y., Gendrin, A., Gondet, B., Poulet, F., Berthé, M., Soufflot, A., Arvidson, R., Mangold, N., Mustard, J., Drossart, P., the OMEGA team, 2005. Mars surface diversity as revealed by the OMEGA/Mars express observations. *Science* 307, 1576–1581.
- Bibring, J.-P., Langevin, Y., Mustard, J.F., Poulet, F., Arvidson, R., Gendrin, A., Gondet, B., Mangold, N., Pinet, P., Forget, F., the OMEGA team, 2006. Global mineralogical and aqueous Mars history derived from OMEGA/Mars express data. *Science* 312, 400–404.
- Christensen, P.R., 2003. Formation of recent Martian gullies through melting of extensive water-rich snow deposits. *Nature* 422, 45–48.
- Clark, R.N., 1981a. Water frost and ice: the near-infrared special reflectance 0.65–2.5 μm. *J. Geophys. Res.* 86, 3087–3096.
- Clark, R.N., 1981b. The spectral reflectance of water-mineral mixtures at low temperatures. *J. Geophys. Res.* 86, 3074–3086.
- Clark, R.N., 1999. Spectroscopy of rocks and minerals and principles of spectroscopy. In: Rencz, A.N. (Ed.), *Manual of Remote Sensing*. John Wiley & Sons, New York.
- Clark, R.N., Roush, T.L., 1984. Reflectance spectroscopy: quantitative analysis techniques for remote sensing application. *J. Geophys. Res.* 89, 6329–6340.
- Clark, R.N., King, T.V.V., Klejwa, M., Swayze, G.A., Vergo, N., 1990. High spectral resolution reflectance spectroscopy of minerals. *J. Geophys. Res.* 95, 12653–12680.
- Cloutis, E.A., Hawthorne, F.C., Mertzman, S.A., Krenn, K., Craig, M.A., Marcino, D., Methot, M., Strong, J., Mustard, J.F., Blaney, D.L., Bell III, J.F., Vilas, F., 2006. Detection and discrimination of sulfate minerals using reflectance spectroscopy. *Icarus* 184, 121–157.
- Costard, F., Forget, F., Mangold, N., Peulvast, J.P., 2002. Formation of recent Martian debris flows by melting of near-surface ground ice at high obliquity. *Science* 295, 110–113.
- Craddock, R.A., Howard, A.D., 2002. The case for rainfall on a warm, wet early Mars. *J. Geophys. Res.* 107, 5111.
- Dalton, J.B., 2003. Spectral behaviour of hydrated sulphate salts: Implications for Europa mission spectrometer design. *Astrobiology* 3, 771–784.
- Direito, M.S., Webb, M.E., 2007. Search for oil reservoirs on Mars. *Int. J. Astrobiology* 6, 62–63.
- Dreibus, G., Waenke, H., 1987. Volatiles on Earth and Mars: a comparison. *Icarus* 71, 225–240.
- Dreibus, G., Waenke, H., 2000. The volatile inventory of Earth and Mars. AGU 2000 Spring Meeting, Washington, DC.
- Fairén, A.G., Dohm, J.M., Baker, V.R., de Pablo, M.A., Ruiz, J., Ferris, J., Anderson, R., 2003. Episodic flood inundations of the northern plains of Mars. *Icarus* 165, 53–67.
- Fan, C., Schulze-Makuch, D., Fairén, A.G., Wolff, J.A., 2008. A new hypothesis for the origin and redistribution of sulfates in the equatorial region of western Mars. *Geophys. Res. Lett.* 35, L06201.
- Gaidos, E.J., 2001. Cryovolcanism and the recent flow of liquid water on Mars. *Icarus* 153, 218–223.
- Gendrin, A., Mangold, N., Bibring, J.-P., Langevin, Y., Gondet, B., Poulet, F., Bonello, G., Quantin, C., Mustard, J., Arvidson, R., LeMouélic, S., 2005. Sulphates in Martian layered terrains: the OMEGA/Mars express view. *Science* 307, 1587–1591.
- Golombek, M.P., 1999. Martian climate: a message from warmer times. *Science* 283, 1470–1471.
- Hartmann, W.K., 2001. Martian seeps and their relation to youthful geothermal activity. *Space Sci. Rev.* 96, 405–410.
- Haskin, L.A., Wang, A., Jolliff, B.L., McSween, H.Y., Clark, B.C., Des Marais, D.J., McLennan, S.M., Tosca, N.J., Hurowitz, J.A., Farmer, J.D., Yen, A., Squyres, S.W., Arvidson, R.E., Klingelhöfer, G., Schröder, C., de Souza Jr., P.A., Ming, D.W., Gellert, R., Zipfel, J., Brückner, J., Bell III, J.F., Herkenhoff, K., Christensen, P.R., Ruff, S., Blaney, D., Gorevan, S., Cabrol, N.A., Crumpler, L., Grant, J., Soderblom, L., 2005. Water alteration of rocks and soils on Mars at the Spirit rover site in Gusev crater. *Nature* 436, 66–69.
- Heldmann, J.L., Mellon, M.T., 2004. Observations of Martian gullies and constraints on potential formation mechanisms. *Icarus* 168, 285–304.
- Heldmann, J.L., Toon, O.B., Pollard, W.H., Mellon, M.T., Pitlick, J., McKay, C.P., Andersen, D.T., 2005. Formation of Martian gullies by the action of liquid water flowing under current Martian environmental conditions. *J. Geophys. Res.* 110, E05004.
- Heldmann, J.L., Carlsson, E., Johansson, H., Mellon, M.T., Toon, O.B., 2007. Observations of Martian gullies and constraints on potential formation mechanisms: II. The northern hemisphere. *Icarus* 188, 324–344.
- Hunt, G.R., Salisbury, J.W., 1970. Visible and near infrared spectra of minerals and rocks, I, silicate minerals. *Mod. Geol.* 2, 283–300.
- Kerr, R.A., 2003. Running water eroded a frigid early Mars. *Science* 300, 1496–1497.
- Langevin, Y., Poulet, F., Bibring, J.-P., Gondet, B., 2005. Sulphates in the north polar region of Mars detected by OMEGA/Mars express. *Science* 307, 1584–1586.
- Langevin, Y., Bibring, J.-P., Montmessin, F., Forget, F., Vincendon, M., Doute, S., Poulet, F., Gondet, B., 2007. Observations of the south seasonal cap of Mars during recession in 2004–2006 by the OMEGA visible/near-infrared imaging spectrometer on board Mars express. *J. Geophys. Res.* 112, E08S12.
- Malin, M.C., Edgett, K.S., 2000a. Evidence for recent groundwater seepage and surface runoff on Mars. *Science* 288, 2330–2335.
- Malin, M.C., Edgett, K.S., 2000b. Sedimentary rocks of early Mars. *Science* 290, 1927–1937.
- Malin, M.C., Edgett, K.S., 2003. Evidence for persistent flow and aqueous sedimentation on early Mars. *Science* 302, 1931–1934.
- Malin, M.C., Edgett, K.S., Posiolova, L.V., McColley, S.M., Dobrea, E.Z.N., 2006. Present-day impact cratering rate and contemporary gully activity on Mars. *Science* 314, 1573–1577.
- Malin Space Science Systems, 2000. Mars Global Surveyor Mars Orbiter Camera Image Gallery. <http://www.msss.com/moc_gallery/>.
- Mangold, N., Quantin, C., Ansan, V., Delacourt, C., Allemand, P., 2004. Evidence for precipitation on Mars from detritic valleys in the Valles Marineris area. *Science* 305, 78–81.
- McCullom, T.M., Hynek, B.M., 2005. A volcanic environment for bedrock diagenesis at Meridiani Planum on Mars. *Nature* 438, 1129–1131.
- McEwen, A.S., Hansen, C.J., Delamere, W.A., Eliason, E.M., Herkenhoff, K.E., Keszthelyi, L., Gulick, V.C., Kirk, R.L., Mellon, M.T., Grant, J.A., et al., 2007. A closer look at water-related geologic activity on Mars. *Science* 317, 1706–1709.
- Mellon, M.T., Phillips, R.J., 2001. Recent gullies on Mars and the source of liquid water. *J. Geophys. Res.* 106, 23165–23179.
- Musselwhite, D.S., Swindle, T.D., Lunine, J.I., 2001. Liquid CO₂ breakout and the formation of recent small gullies on Mars. *Geophys. Res. Lett.* 28, 1283–1286.
- Paige, D.A., 2005. Ancient Mars: wet in many places. *Science* 307, 1575–1576.
- Parker, T.J., Saunders, R.S., Schneeberger, D.M., 1989. Transitional morphology in west Deuteronilus Mensae, Mars: implications for modifications of the lowland/upland boundary. *Icarus* 82, 111–145.
- Pelletier, J.D., Kolb, K.J., McEwen, A.S., Kirk, R.L., 2008. Recent bright gully deposits on Mars: wet or dry flow? *Geology* 36, 193–272.
- Pollack, J.B., Kasting, J.F., Richardson, S.M., Poliakov, K., 1987. The case for a wet, warm climate on early Mars. *Icarus* 71, 203–224.
- Poulet, F., Bibring, J.-P., Mustard, J.F., Gendrin, A., Mangold, N., Langevin, Y., Arvidson, R.E., Gondet, B., Gomez, C., 2005. Phyllosilicates on Mars and implications for early Martian climate. *Nature* 438, 623–627.
- Reiss, D., Jaumann, R., 2003. Recent debris flows on Mars: seasonal observations of the Russell Crater dune field. *Geophys. Res. Lett.* 30.
- Rossman, G.R., 1975. Spectroscopic and magnetic studies of ferric iron hydroxyl sulphates: intensification of colour in ferric iron clusters bridged by a single hydroxide ion. *Am. Mineral.* 60, 698–704.
- Sagan, C., Toon, O.B., Gierasch, P.J., 1973. Climatic change on Mars. *Science* 181, 1045–1049.
- Schorghofer, N., Edgett, K.S., 2006. Seasonal surface frost at low latitudes on Mars. *Icarus* 180, 321–334.
- Schulze-Makuch, D., Irwin, L.N., 2004. *Life in the Universe: Expectations and Constraints*. Springer, Berlin.
- Schulze-Makuch, D., Dohm, J.M., Fan, C., Fairén, A.G., Rodriguez, J.A.P., Baker, V.R., Finkert, W., 2007. Exploration of hydrothermal targets on Mars. *Icarus* 189, 308–324.
- Soare, R.J., Kargel, J.S., Osinski, G.R., Costard, F., 2007. Thermokarst processes and the origin of crater-rim gullies in Utopia and western Elysium Planitia. *Icarus* 191, 92–112.
- Solomon, S.C., Aharonson, O., Aurnou, J.M., Banerdt, W.B., Carr, M.H., Dombard, A.J., Frey, H.V., Golombek, M.P., Hauck II, S.A., Head III, J.W., Jakosky, B.M., Johnson, C.L., McGovern, P.J., Neumann, G.A., Phillips, R.J., Smith, D.E., Zuber, M.T., 2005. New perspectives on ancient Mars. *Science* 307, 1214–1220.
- Squyres, S.W., Kasting, J.F., 1994. Early Mars: how warm and how wet? *Science* 265, 744–749.
- Squyres, S.W., Grotzinger, J.P., Arvidson, R.E., Bell III, J.F., Calvin, W., Christensen, P.R., Clark, B.C., Crisp, J.A., Farrand, W.H., Herkenhoff, K.E., Johnson, J.R., Klingelhöfer, G., Knoll, A.H., McLennan, S.M., McSween Jr., H.Y., Morris, R.V., Rice Jr., J.W., Rieder, R., Soderblom, L.A., 2004. In situ evidence for an ancient aqueous environment at Meridiani Planum, Mars. *Science* 306, 1709–1714.
- Sullivan, R., Thomas, P., Veverka, J., Malin, M., Edgett, K.S., 2001. Mass movement slope streaks imaged by the Mars orbiter camera. *J. Geophys. Res.* 106, 23607–23634.
- Svitek, T., Murray, B., 1990. Winter Frost at the Viking Lander 2 site. *J. Geophys. Res.* 95, 1495–1510.
- Tanaka, K.L., 2000. Fountains of youth. *Science* 288, 2325.
- Treiman, A.H., 2003. Geologic settings of Martian gullies: implications for their origins. *J. Geophys. Res.* 108 (E4).